A self-sustaining ultrahigh-frequency nanoelectromechanical oscillator

X. L. FENG[1,2], C. J. WHITE[2], A. HAJIMIRI[2] AND M. L. ROUKES[1]*

[1]Kavli Nanoscience Institute, MC 114-36, California Institute of Technology, Pasadena, California 91125, USA
[2]Electrical Engineering, MC 136-93, California Institute of Technology, Pasadena, California 91125, USA
*e-mail: roukes@caltech.edu

Published online: 25 May 2008; doi:10.1038/nnano.2008.125

Sensors based on nanoelectromechanical systems vibrating at high and ultrahigh frequencies[1] are capable of levels of performance that surpass those of larger sensors. Nanoelectromechanical devices have achieved unprecedented sensitivity in the detection of displacement[2], mass[3], force[4] and charge[5]. To date, these milestones have been achieved with passive devices that require external periodic or impulsive stimuli to excite them into resonance. Here, we demonstrate an autonomous and self-sustaining nanoelectromechanical oscillator that generates continuous ultrahigh-frequency signals when powered by a steady d.c. source. The frequency-determining element in the oscillator is a 428 MHz nanoelectromechanical resonator that is embedded within a tunable electrical feedback network to generate active and stable self-oscillation. Our prototype nanoelectromechanical oscillator exhibits excellent frequency stability, linewidth narrowing and low phase noise performance. Such ultrahigh-frequency oscillators provide a comparatively simple means for implementing a wide variety of practical sensing applications. They also offer intriguing opportunities for nanomechanical frequency control, timing and synchronization.

Active oscillators spontaneously generate self-sustaining periodic signals by extracting power from steady (d.c.) sources. This distinguishes them from passive resonators—which are characterized, in contrast, by a damped response to impulsive stimuli—and makes them invaluable for applications in precision timekeeping[6], communications[7] and sensing[8], which require continuous a.c. signals. Oscillators based upon the mechanical vibrations of crystals such as quartz resonators have long been ubiquitous in electronics, as a result of their simplicity and excellent stability for frequency control applications[9]. Over the past few decades, there has been considerable incentive to miniaturize such mechanical resonators, in order to integrate them on-chip with electronic components to add frequency-selection and tuning elements[10,11]. In particular, it is desirable to realize highly accurate and stable clocks or frequency references with integrated, chip-based systems using miniaturized acoustically resonant devices.

Resonant nanoelectromechanical systems (NEMS) have recently generated significant interest in this area because of their ultrahigh operating frequencies[1], small size, very low operating power and high quality factors (Q). In fact, the values of Q achieved by NEMS typically greatly exceed what can be obtained using electronic components. In parallel with the quest for miniaturized frequency references, which motivates the development of nanoscale resonators, efforts are particularly focused on exploiting their unprecedented responsivity for a variety of sensing applications in science and technology[2–5]. Accordingly, there is significant impetus for developing self-sustaining NEMS oscillators for ultrasensitive, frequency-shift-based sensing. However, for reasons we describe below, ultrahigh-frequency (UHF; $\geq$300 MHz) signal generation based on nanoscale devices has remained elusive, despite recent advances in the development of high-frequency, microelectromechanical systems (MEMS) oscillators[12,13]. Here, for the first time, we harness the fundamental-mode vibrations of a nanoscale mechanical device to obtain stable, self-sustaining oscillations at UHF—at fundamental frequencies significantly higher than typically achieved with conventional quartz crystal oscillators ($\sim$10 MHz) or with the recently developed MEMS oscillators (up to $\sim$60 MHz)[13].

Our self-sustaining NEMS oscillator, as shown in Fig. 1a, consists of an electrical feedback circuit with an embedded UHF NEMS resonator as the frequency-determining element. This element's motion is transduced into an electrical signal, amplified, and then fed back (with adjustable gain and phase) to the NEMS resonator. Stable mechanical vibration of the NEMS element is maintained with d.c. power input to the amplifier in this feedback loop. The elusiveness of successfully producing UHF and microwave-frequency oscillators based on NEMS stems from the difficulty in obtaining optimal transduction of their miniscule displacements. After transduction into the electrical domain, the motion-induced signals generated by such scaled-down resonators are extremely small, making them exceptionally difficult to tune and control in an electrical feedback circuit. Specifically, the unavoidable parasitic coupling between a NEMS device and its macroscale surroundings generally overwhelms its intrinsic electromechanical response. We overcome this with a precisely tunable detection circuit (see Supplementary Information) that deeply nulls the unavoidable parasitics, to allow transduction of UHF NEMS vibratory motions into electrical signals with high efficiency. For a doubly clamped silicon carbide (SiC) beam with dimensions 1.65 μm (L) $\times$ 120 nm (w) $\times$ 80 nm (t), and a fundamental flexural mode resonance of $\omega_0/2\pi = 428.2$ MHz and $Q \sim 2{,}500$, this enables us to achieve a resonant, open-loop electrical response that is 8 dB above the background. (See Methods and Supplementary Information for details about device fabrication, resonator displacement transduction, electronic detection circuitry and measurements.)

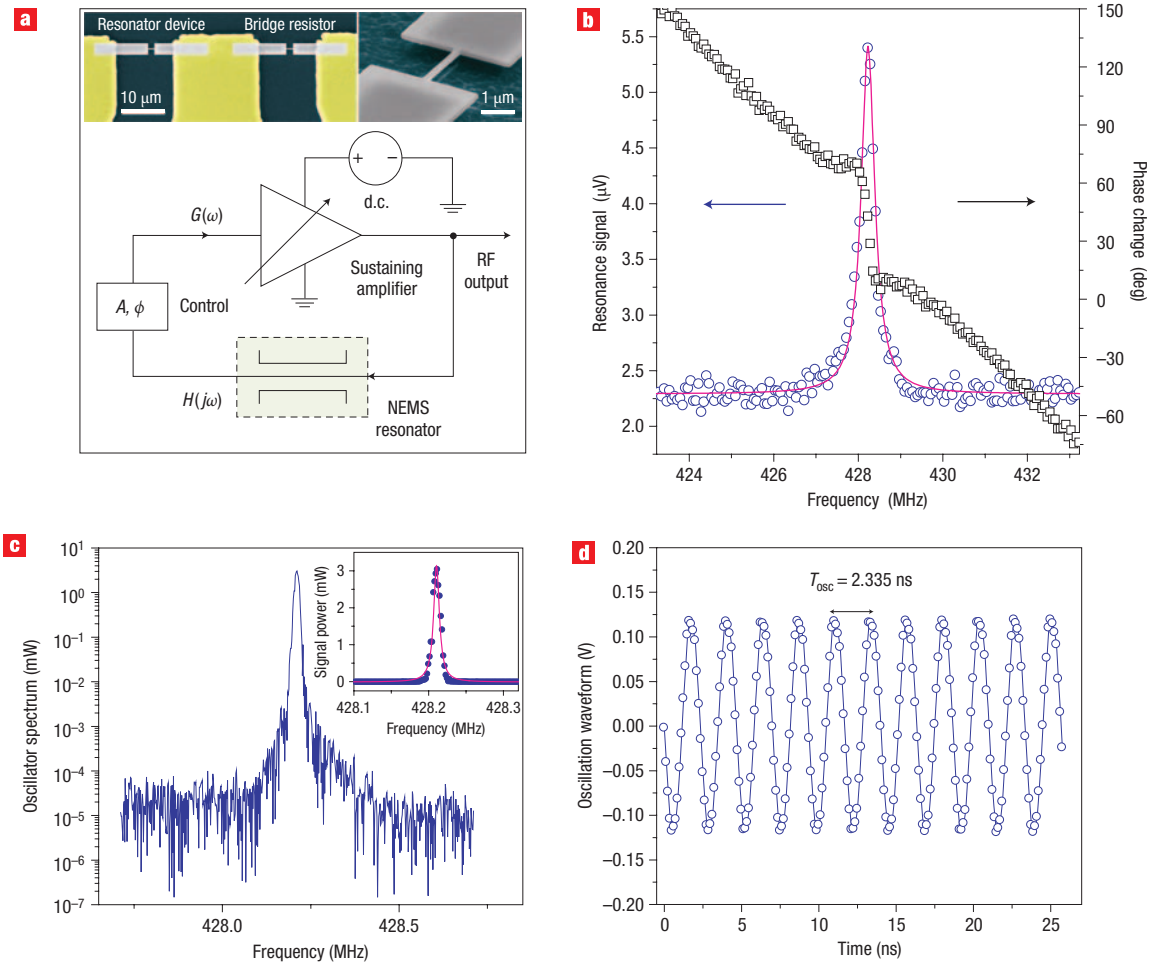

Figure 1 Self-sustaining UHF NEMS oscillator. a, Simplified circuit schematic (see Supplementary Information, Fig. S1, for more detail) for the self-sustaining oscillator, which includes the frequency-determining UHF NEMS resonator and the tunable electronic feedback loop. The inset shows scanning electron micrographs depicting the device (right) and its embedding electrical-bridge configuration (left), from which a large resonant response is obtained by efficiently nulling parasitic signals. **b**, Open-loop electrical-domain amplitude (blue open circles) and phase (black open squares) signals from the 428 MHz NEMS resonator (referred to the input of the preamplifier). A large coherent response 8 dB above the background is observed. The magenta line is a fit of the signal amplitude to the model for a damped driven harmonic resonator. **c**, Output power spectrum of the NEMS oscillator (on a logarithmic scale) as a function of frequency measured with a 100 kHz resolution bandwidth. The inset shows the output power spectrum on a linear scale: the linewidth narrowing can be clearly seen (as compared with Fig. 1b). **d**, The clean, stable, sinusoidal time-domain oscillation waveform of the closed-loop NEMS oscillator measured by a high-speed digital oscilloscope.

To realize a NEMS-based oscillator, it is critical to obtain a clean resonant response well above the background over a wide frequency range (Fig. 1b). Under such conditions, it becomes possible to calibrate and adjust the open-loop gain and phase changes to satisfy the Barkhausen criterion[7], $G(\omega_0)H(j\omega_0) = 1$, on resonance, $\omega = \omega_0$. Here, $G(\omega)$ is the gain of the feedback loop and $H(j\omega)$ the transfer function of the frequency-determining NEMS element; we represent both as complex functions. Fulfilling the Barkhausen condition ensures that the electronic feedback exactly compensates the nanoresonator's intrinsic and extrinsically coupled damping, thereby sustaining continuous oscillation. This requires precise tuning of the loop gain and phase. In the steady state, the amplitude of oscillation is stabilized by nonlinearity in the electronic gain, $G(\omega)$, at large signal amplitudes. The steady-state self-oscillations of the system are readily characterized by the frequency-domain power spectrum of the oscillator output (Fig. 1c). Figure 1d demonstrates the clean, stable, time-domain oscillation waveforms from the output of the closed-loop NEMS oscillator, displaying a period of $T_{osc} = 2.335$ ns.

A compelling feature of the NEMS oscillator is the linewidth narrowing[14] in its frequency-domain spectrum when compared with that of the passive resonator. The driven resonator's response has a lorentzian line broadening (Fig. 1b) due to its damping (finite Q), and the linewidth, set by the damping rate, is $\Delta_{res} = \omega_0/(2\pi Q_{res}) \approx 0.1713$ MHz. Following the same convention of full-width at half-maximum (FWHM) of the power signal, the linewidth of the NEMS oscillator is measured to be $\Delta_{osc} \equiv \text{FWHM} \approx 9$ kHz. The linewidth narrowing ratio is $\Delta_{osc}/\Delta_{res} \approx 1/19$, which corresponds to an effective Q factor of $Q_{osc,eff} = \omega_0/(2\pi\Delta_{osc}) \approx 47{,}580$ for the oscillator. The inset of Fig. 1c approximately illustrates the oscillator linewidth narrowing with a brute-force lorentzian fit to the oscillator power signal. Note here that the oscillator spectrum is strictly lorentzian

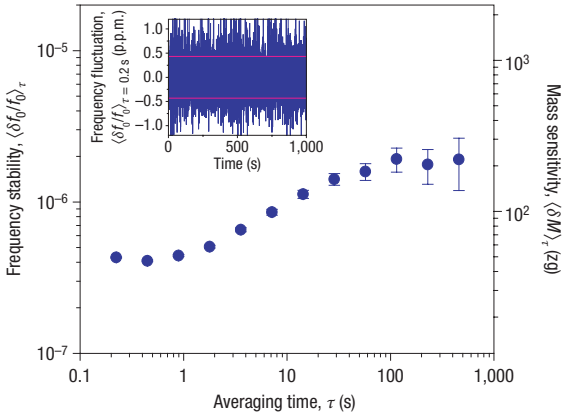

Figure 2 Frequency stability and mass sensitivity of the self-sustaining UHF NEMS oscillator. Measured frequency stability $\langle \delta f_0/f_0 \rangle_\tau$ (on a logarithmic scale) as a function of averaging time τ. The inset shows the 'instantaneous' fractional frequency fluctuation (on a linear scale in units of parts per million of $\sim 4 \times 10^{-7}$ for $\tau = 0.2$ s. This stability level is achieved for short-term averaging, for example, $\tau = 0.2-1$ s. This plot also shows the UHF NEMS oscillator's corresponding mass sensitivity, $\langle \delta M \rangle_\tau \approx 2M_{\text{eff}} \langle \delta f_0/f_0 \rangle_\tau$, again as a function of averaging time τ. Given the NEMS device's active mass of $M_{\text{eff}} = 57.8$ fg, the system achieves a short-term mass resolution of $\sim$50 zg.

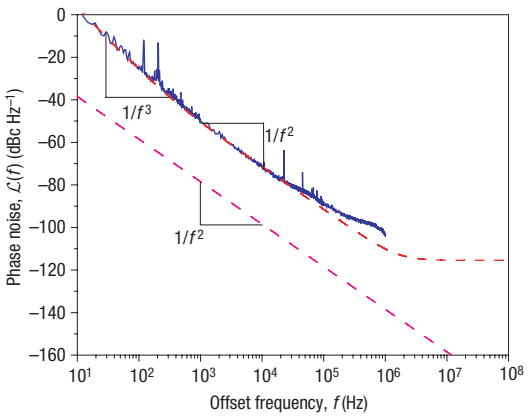

Figure 3 Phase noise performance of the self-sustaining UHF NEMS oscillator. The blue solid line is the measured phase noise data, demonstrating a $1/f^2$ power law and thus thermal-noise-limited performance in most of the frequency range of interest. A Leeson-type empirical fit (red dashed line) further demonstrates that, close to the carrier for offset frequency $f < 300$ Hz, the phase noise approximately follows a $1/f^3$ power law as flicker noise arises in this range. The carrier signal power is $P_C \approx 0.32$ nW. The achieved phase noise performance is presently limited by extrinsic electronic noise from the preamplifier and the NEMS transducer. The ultimate phase noise (magenta dashed line) is limited by thermomechanical fluctuations in the NEMS device, which could be approached by further engineering of the transduction and electronic detection.

when the system noise is white. In this case the oscillator phase noise is a diffusive process, which can be equivalently viewed as a virtual damping effect[14] causing a finite spectral linewidth, similar to the resonator case. When the noise spectral density is not white, the oscillator power signal deviates from lorentzian and such a fit is only an approximation. Nonetheless, one can still estimate Δ_{osc} and $Q_{\text{osc,eff}}$ by using the FWHM.

The frequency stability of our prototype NEMS oscillator is particularly noteworthy. For frequency-shift sensing applications, frequency-fluctuation noise imposes an ultimate limit to detection sensitivity. We characterize the NEMS oscillator's frequency stability by its fractional frequency fluctuations, $\langle \delta f_0/f_0 \rangle_\tau$, which are a function of averaging time τ, $\langle \delta f_0/f_0 \rangle_\tau = [(1/(N-1)) \cdot \sum_{i=1}^{N}((\bar{f}_{i+1} - \bar{f}_i)/f_0)^2]^{1/2}$, where $\bar{f}_i$ is the averaged frequency in the ith discrete time interval of τ. As shown in Fig. 2, we have achieved $\langle \delta f_0/f_0 \rangle_\tau \approx 4 \times 10^{-7}$ for short times ($\tau < 1$ s) and $\sim 1 \times 10^{-6}$ for longer times ($\tau > 100$ s). Such frequency stability is particularly promising for mass sensing: recent advances with ultraminiature mechanical vibratory sensors have yielded unprecedented zeptogram-scale mass sensitivity for applications in vacuum[3] and at atmospheric pressure[15], and attogram sensitivity for fluidic-based sensing[16]. The NEMS oscillator described here—with an active resonator mass M_{eff} of only 57.8 fg and high mass responsivity[17] of $|\Re| = \omega_0/(2M_{\text{eff}}) = 3.7$ Hz zg^{-1}—permits a mass resolution $\langle \delta M \rangle_\tau \approx 2M_{\text{eff}} \langle \delta f_0/f_0 \rangle_\tau$ at the $\sim$50 zg level with short averaging times, $\tau \sim 1-1{,}000$ ms. This is a trillion-fold improvement over typical commercial quartz crystal microbalances[8,18]. The prototype NEMS oscillator is also readily applicable for ultrasensitive force detections in real time[4]. The present 428 MHz doubly clamped beam device has a relatively large stiffness of $k_{\text{eff}} = 418$ N m^{-1} and a fundamental force sensitivity of $S_F^{1/2} = (4k_B T M_{\text{eff}} \omega_0/Q)^{1/2} \approx 275$ aN Hz$^{-1/2}$, limited by its thermomechanical motion. Here k_B is the Boltzmann constant and T the temperature. Combined with cantilever devices of high Q values and lower force constants specifically designed for force sensing[4,19], NEMS oscillators can attain much higher force sensitivities (in the low- and sub-attonewton regimes) while providing wide bandwidth operation[20].

Understanding and minimizing oscillator phase noise is key to attaining high precision and stability. Phase noise is traditionally quantified as the sideband power spectral density at an offset frequency f, normalized by the carrier signal power P_C (the power sustains the resonator's motion). This is written as $\mathcal{L}(f) = 10 \log[P_{\text{sideband}}(f_C + f)/P_C]$, and has units of dBc Hz^{-1} (decibels below the carrier per hertz)[7,14,21]. As shown in Fig. 3, the measured phase noise spectrum of the prototype UHF NEMS oscillator closely follows a $1/f^2$ power law in the 300 Hz to 1 MHz offset frequency range. This indicates that phase noise in this regime originates predominantly from fluctuating sources with white spectra[14,21]. In the present case, these are largely the electronic thermal noise from the NEMS displacement transducer and its readout amplifier. Close in to the resonance peak frequency (carrier), we observe phase noise exhibiting $1/f^3$ behaviour, which is consistent with $1/f$ (flicker) noise mechanisms expected in this regime. As Fig. 3 displays, we find that an empirical fit to a Leeson-type model[21,22]—that is, $\mathcal{L}(f) = 10 \log[(2F_n k_B T/P_C) \cdot (1 + (f_0/2Qf))^2(1 + (f_{1/f^3}/f))]$—agrees very well with the measured phase noise data. This fit yields an equivalent noise factor of $F_n = 1.4$ and corner (knee) offset frequency for $1/f^3$ phase noise (that is, $1/f$ frequency noise) of $f_{1/f^3} \approx 300$ Hz. The time-domain oscillation stability and frequency-domain phase noise are correlated, as can be seen in Figs 2 and 3. Whereas white and flicker noise affect the short term performance, it is drift and aging that compromise the oscillator's long-term stability. From measurements and analyses of the oscillator's phase fluctuations (see Methods and Supplementary Information), we deduce that the combination of electrical-domain thermal noise in the transducer and loop amplifier dominates the mechanical-domain noise of the NEMS

resonator itself in this oscillator realization. Note that, for communications applications, the phase noise performance of the prototype NEMS oscillator needs further engineering (for example, in improving the device carrier power P_C). MEMS oscillators based upon micromachined devices operating in much stiffer (for example, bulk acoustic) modes[13,23], although not optimal for sensing applications, are now approaching the phase noise specifications of macroscale quartz crystal oscillators[24]. Further miniaturization of film-bulk acoustic resonators (FBARs)[23] and devices using other stiff modes, and arraying ensembles of devices, should significantly enhance the power handling and phase noise performance of NEMS oscillators.

The ultimate limits of phase noise performance are imposed by the NEMS resonator's intrinsic thermomechanical fluctuations[25]. The corresponding phase noise in this limit is $\mathcal{L}(f) = 10\log[(k_BT/2P_CQ^2)\cdot(f_0/f)^2]$, which is also displayed in Fig. 3. We can also represent this limit by its corresponding fractional frequency fluctuations, again as a function of averaging time τ, $\langle\delta f_0/f_0\rangle_\tau = (1/Q)\cdot(\pi k_BT/P_C\tau)^{1/2}$. For the NEMS device in this work, this yields an ultimate limit of $\langle\delta f_0/f_0\rangle_\tau \approx 5\times10^{-10}$ for $\tau\sim1$ s. Hence, with further optimization, up to a thousand-fold improvement in performance may be possible over our present extrinsic-noise-limited value, $\langle\delta f_0/f_0\rangle_\tau \approx 4\times10^{-7}$ for $\tau = 1$ s.

Self-sustaining NEMS oscillators enable a wide spectrum of applications. They offer significant advantages over previously used methods of frequency-shift detection (for example, phase-locked loops[3,15]) as no source of external excitation is required. This yields an immense simplification of design that is crucial for next-generation, highly multiplexed sensing applications involving large arrays of devices. Additionally, NEMS oscillators will enable important applications in metrology at the nanoscale, providing a generic approach to wideband and real-time transduction of fundamental physical processes[26]. Furthermore, large arrays of coupled tunable mechanical oscillators may offer promising prospects for nanomechanical timing, signal processing[27] and noise suppression through oscillator synchronization[28]. It should be noted that synchronization requires the coupling of self-sustaining, autonomous oscillators, rather than passive resonators[29]. Arrays of NEMS oscillators may also provide an intriguing means of simulating biological systems, such as pacemaker cells and neural oscillators[30], where large numbers of oscillators spontaneously synchronize to perform collective functions.

METHODS

FABRICATION AND DETECTION OF UHF NEMS RESONATORS

We fabricated the UHF NEMS resonators from an 80-nm single-crystal SiC epilayer grown upon a silicon substrate, using a surface nanomachining process as detailed elsewhere[31]. In brief, for the structures shown in the insets to Fig. 1a, the contacting gold electrodes were defined by photolithography, deposition of a 80-nm gold layer and a liftoff process. The NEMS devices were successively defined by e-beam lithography, metallized by a thermally evaporated ~5–10-nm layer of titanium on top of ~30–40-nm aluminium, and then a liftoff process. The metallization was engineered so that the device's two-terminal resistance was typically ~100 Ω at room temperature and ~50 Ω at low temperatures to facilitate electronic characterization at UHF.

The device's fundamental, in-plane, flexural mode resonance was excited and detected using magnetomotive transduction, which we find is particularly suitable for doubly clamped beam resonators in the UHF range[1,31]. Measurements were carried out in vacuo, with the NEMS resonator regulated at a temperature of $T = 22$ K and immersed in an 8 T magnetic field. Note that although magnetomotive transduction is probably the most successful scheme for UHF nanobeam or nanowire resonators to date that does not require frequency downconversion, it should not be taken as a fundamental or intrinsic ingredient for UHF NEMS. Efficient actuation and wideband sensitive detection are being actively pursued through the adoption of new materials and nanomechanical coupling effects[32,33] and new circuit techniques, to enable integrated, room-temperature transduction of UHF nanobeams and nanowires.

Here, electronic displacement detection was optimized through the use of a tunable, high-resolution bridge circuit to deeply null the background response arising from parasitic effects, impedance mismatch, and so on, to yield excellent signal-to-background ratios (SBRs) of the order of ~5–10 dB, on resonance (see Supplementary Information, Fig. S1). This is unprecedented in the detection of UHF NEMS resonators and is a significant improvement over the typical ~0.1 dB (or even smaller) SBRs previously achieved with UHF NEMS devices[1,31].

UHF NEMS DETECTION NOISE AND OSCILLATOR PHASE NOISE

The electrically transduced NEMS resonator can be represented by its d.c. resistance in series with its electromechanical impedance (see Supplementary Information, Fig. S1). The latter is modelled by a parallel $R_mC_mL_m$ electrical resonator[34]. Here, the subscript m denotes that these arise from the resonator's motion. Note that the series resonant circuit model for capacitive transduction[13] widely used in MEMS often involves a very large motional resistance (typically in the kΩ to MΩ ranges). Here, our NEMS devices are described by a parallel resonant circuit model and are close to 50 Ω in total impedance. This is more suitable for UHF in terms of impedance matching in transduction and choice of sustaining amplifiers. The detection noise floor reached in these experiments is limited by the post-transducer amplifier's voltage noise (with a calibrated noise temperature of $T_n = 9$ K) in combination with Johnson noise of the series d.c. resistance. This combination yields a total voltage noise of ~0.238 nV Hz$^{-1/2}$ (referred to the input of the preamplifier). This translates into an effective displacement sensitivity of ~12.8 fm Hz$^{-1/2}$. At $T = 22$ K, the ultimate limit to the displacement noise floor for this device is set by thermomechanical fluctuations and corresponds to ~1.64 fm Hz$^{-1/2}$. This thermomechanical motion generates, in the presence of the 8 T magnetic field, an equivalent electromotive-force voltage noise floor of ~0.0305 nV Hz$^{-1/2}$. The onset of nonlinearity arising from the Duffing instability[35] for this device is ~1.6 nm, so the device possesses an intrinsic dynamic range[35] of 114 dB. However, in these experiments the bottom-most 18 dB of the intrinsic dynamic range is forfeited due to the imperfect noise match between the transducer and the subsequent readout amplifier, as described above. The dynamic range available to the system, including both the NEMS resonator and detection circuitry, is therefore about 96 dB.

For the self-sustaining NEMS oscillator, the total phase noise can be viewed as the sum of several parts. First, fluctuations associated with the vibration-induced motional resistance, $R_m \sim 1.5$ Ω, appearing in the parallel $R_mC_mL_m$ representation of the NEMS electromechanical impedance (see Supplementary Information, Fig. S1), correspond to the thermomechanical displacement noise of the resonator transduced into the electrical domain. In this domain, additional electrical noise originates from the d.c. resistance of the transducer, which we model as an equivalent series resistance $R_{S,eq} = 26.1$ Ω. Under the conditions of this experiment $R_{S,eq} > R_m$, so optimal engineering can further improve the measured noise floor.

Received 14 February 2008; accepted 16 April 2008; published 25 May 2008.

References

1. Huang, X. M. H., Zorman, C. A., Mehregany, M. & Roukes, M. L. Nanodevice motion at microwave frequencies. *Nature* **421,** 496 (2003).
2. LaHaye, M. D., Buu, O., Camarota, B. & Schwab, K. C. Approaching the quantum limit of a nanomechanical resonator. *Science* **304,** 74–77 (2004).
3. Yang, Y. T., Callegari, C., Feng, X. L., Ekinci, K. L. & Roukes, M. L. Zeptogram-scale nanomechanical mass sensing. *Nano Lett.* **6,** 583–586 (2006).
4. Rugar, D., Budakian, R., Mamin, H. J. & Chui, B. W. Single spin detection by magnetic resonance force microscopy. *Nature* **430,** 329–332 (2004).
5. Cleland, A. N. & Roukes, M. L. A nanometre-scale mechanical electrometer. *Nature* **392,** 160–162 (1998).
6. Audoin, C. & Guinot, B. *The Measurement of Time: Time, Frequency, and the Atomic Clock* (trans. Lyle, S.) (Cambridge Univ. Press, New York, 2001).
7. Hajimiri, A. & Lee, T. H. *The Design of Low Noise Oscillators* (Kluwer Academic Publishers, Norwell, 1999).
8. Ward, M. D. & Buttry, D. A. In situ interfacial mass detection with piezoelectric transducers. *Science* **249,** 1000–1007 (1990).
9. Cady, W. G. The piezo-electric resonator. *Proc. IRE* **10,** 83–114 (1922).
10. Nathanson, H. C., Newell, W. E., Wickstrom, R. A. & Davis, J. R. Jr. The resonant gate transistor. *IEEE Trans. Electron. Dev.* **ED-14,** 117–133 (1967).
11. Newell, W. E. Miniaturization of tuning forks. *Science* **161,** 1320–1326 (1968).
12. Nguyen, C. T. C. & Howe, R. T. An integrated CMOS micromechanical resonator high-*Q* oscillator. *IEEE J. Solid State Circ.* **34,** 440–455 (1999).

13. Lin, Y. W. *et al.* Series-resonant VHF micromechanical resonator reference oscillators. *IEEE J. Solid State Circ.* **39,** 2477–2491 (2004).
14. Ham, D. & Hajimiri, A. Virtual damping and Einstein relation in oscillators. *IEEE J. Solid State Circ.* **38,** 407–418 (2003).
15. Li, M., Tang, H. X. & Roukes, M. L. Ultra-sensitive NEMS-based cantilevers for sensing, scanned probe and very high-frequency applications. *Nature Nanotech.* **2,** 114–120 (2007).
16. Burg, T. P. *et al.* Weighing of biomolecules, single cells and single nanoparticles in fluid. *Nature* **446,** 1066–1069 (2007).
17. Ekinci, K. L., Yang, Y. T. & Roukes, M. L. Ultimate limits to inertial mass sensing based upon nanoelectromechanical systems. *J. Appl. Phys.* **95,** 2682–2689 (2004).
18. Rodahl, M., Höök, F., Krozer, A., Brzezinski, P. & Kasemo, B. Quartz crystal microbalance setup for frequency and Q-factor measurements in gaseous and liquid environments. *Rev. Sci. Instrum.* **66,** 3924–3930 (1995).
19. Arlett, J. L., Maloney, J. R., Gudlewski, B., Muluneh, M. & Roukes, M. L. Self-sensing micro- and nanocantilevers with attonewton-scale force resolution. *Nano Lett.* **6,** 1000–1006 (2006).
20. Albrecht, T. R., Grütter, P., Horne, D. & Rugar, D. Frequency modulation detection using high-*Q* cantilevers for enhanced force microscope sensitivity. *J. Appl. Phys.* **69,** 668–673 (1991).
21. Lee, T. H. & Hajimiri, A. Oscillator phase noise: a tutorial. *IEEE J. Solid State Circ.* **35,** 326–336 (2000).
22. Leeson, D. B. A simple model of feedback oscillator noise spectrum. *Proc. IEEE* **54,** 329–330 (1966).
23. Otis, B. P. & Rabaey, J. M. A 300 μW 1.9 GHz CMOS oscillator utilizing micromachined resonators. *IEEE J. Solid State Circ.* **38,** 1271–1274 (2003).
24. Vig, J. R. & Kim, Y. Noise in microelectromechanical system resonators. *IEEE Trans. Ultrason. Ferroelectr. Freq. Contr.* **46,** 1558–1565 (1999).
25. Cleland, A. N. & Roukes, M. L. Noise processes in nanomechanical resonators. *J. Appl. Phys.* **92,** 2758–2769 (2002).
26. Schwab, K. C. & Roukes, M. L. Putting mechanics into quantum mechanics. *Phys. Today* **58,** 36–42 (July 2005).
27. Nguyen, C. T. C., Katehi, L. P. B. & Rebeiz, G. M. Micromachined devices for wireless communications. *Proc. IEEE* **86,** 1756–1768 (1998).
28. Cross, M. C., Zumdieck, A., Lifshitz, R. & Rogers, J. L. Synchronization by nonlinear frequency pulling. *Phys. Rev. Lett.* **93,** 224101 (2004).
29. Pikovsky, A., Rosenblum, M. & Kurths, J. *Synchronization: A Universal Concept in Nonlinear Sciences* (Cambridge Univ. Press, 2001).
30. Varela, F., Lachaux, J. P., Rodriguez, E. & Martinerie, J. The brainweb: phase synchronization and large-scale integration. *Nature Rev. Neurosci.* **2,** 229–239 (2001).
31. Huang, X. M. H., Feng, X. L., Zorman, C. A., Mehregany, M. & Roukes, M. L. VHF, UHF and microwave frequency nanomechanical resonators. *New J. Phys.* **7,** 247 (2005).
32. Lin, Y. W., Li, S. S., Xie, Y., Ren, Z. & Nguyen, C. T. C. Vibrating micromechanical resonators with solid dielectric capacitive transducer gaps, in *Proc. IEEE Int. Freq. Contr. Symp.*, August 29–31, 128–134 (IEEE, Vancouver, Canada, 2005).
33. Masmanidis, S. C. *et al.* Multifunctional nanomechanical systems via tunably coupled piezoelectric actuation. *Science* **317,** 780–783 (2007).
34. Cleland, A. N. & Roukes, M. L. External control of dissipation in a nanometer-scale radiofrequency mechanical resonator. *Sens. Actuators A* **72,** 256–261 (1999).
35. Postma, H. W. C., Kozinsky, I., Husain, A. & Roukes, M. L. Dynamic range of nanotube- and nanowire-based electromechanical systems. *Appl. Phys. Lett.* **86,** 223105 (2005).

Supplementary Information accompanies this paper at www.nature.com/naturenanotechnology.

Acknowledgements

We thank C.T.C. Nguyen, J.R. Vig, M.C. Cross and R. Lifshitz for helpful discussions. We thank M. Mehregany and C.A. Zorman for providing SiC material. We acknowledge support from DARPA/SPAWAR under grant N66001-02-1-8914.

Author information

Reprints and permission information is available online at http://npg.nature.com/reprintsandpermissions/.
Correspondence and requests for materials should be addressed to M.L.R.

Online Supplementary Information

A Self-Sustaining Ultra High Frequency Nanoelectromechanical Oscillator

X.L. Feng[1,2], C.J. White[2], A. Hajimiri[2], M.L. Roukes[1*]

[1]Kavli Nanoscience Institute, MC 114-36, and [2]Electrical Engineering, MC 136-93
California Institute of Technology, Pasadena, CA 91125, USA

[*]E-mail: roukes@caltech.edu

From Open-Loop UHF NEMS Resonance Detection to Close-Loop Self Oscillation

Fig. S1 shows the circuit diagram for a self-sustaining UHF NEMS oscillator. As shown, open-loop measurements in the resonance-detection mode are made via two-port network analysis (transmission from port 1 to port 2) by employing a UHF/microwave network analyzer (HP8720C).

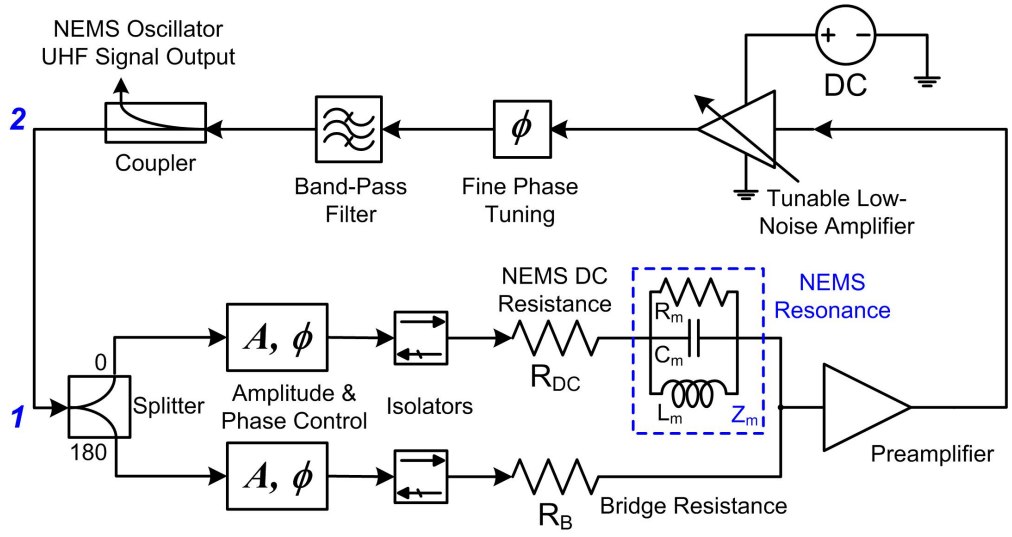

Figure S1 Circuit diagram for the demonstration and characterization of a self-sustaining UHF NEMS oscillator.

In open-loop operation, this finely-tunable bridge circuit[S1] can deeply null the background response arising from parasitic effects and impedance mismatch to yield excellent signal-to-background ratios (SBR's) of order ~5−10dB, on resonance. Various components for high-resolution 180-degree-phase bridging and background nulling are also illustrated in the circuit diagram. Here R_B is the resistance of a nanofabricated bridge resistor on chip (as shown in the inset of Fig. 1) – in practice it is often more convenient to employ another metalized nanobeam whose DC resistance is very close to the DC resistance of the resonator device of interest. This

bridge nanobeam has also been made so that its resonance frequency is far enough from the resonance frequency of the resonator device of interest. Parasitic reflection and standing wave effects due to mismatch are efficiently reduced via directional signal isolation. Amplitude and phase in each branch of the bridge are precisely controlled by high-precision attenuators and delay lines. Both the loop gain and phase change can be finely tuned.

As demonstrated in Fig. S2, typical open-loop measurements of the UHF NEMS responses employing the circuit in Fig. S1 can yield SBR's of ~10dB. This represents a significant improvement over the SBR's of ~0.1–0.5dB typically obtained with the previous scheme[S2,S3].

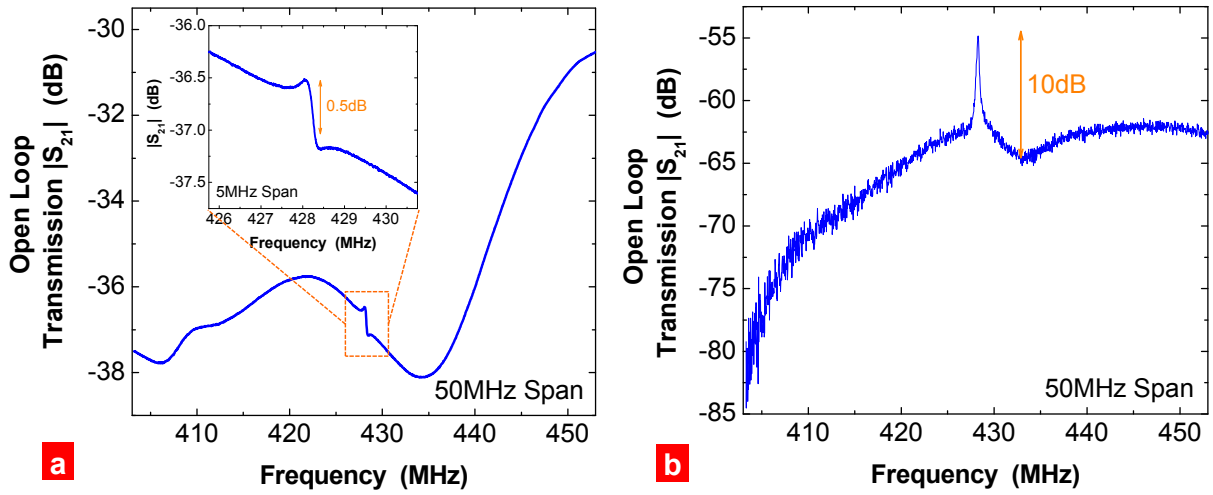

Figure S2 Open loop measurement of UHF NEMS resonance response (transmission $|S_{21}|$ between the nodes 1 and 2). **(a)** Small UHF resonance signal embedded in large, complex background response, measured by employing the scheme and circuit used in references [S2] and [S3]. **(b)** Significantly enhanced UHF resonance signal measured using the circuit shown in Fig. S1 in its open-loop mode (before applying feedback gain).

Self-Sustaining UHF NEMS Oscillator Characterization

Fig. S3 demonstrates the open-loop calibration and adjustment of the loop gain and loop phase change to enable attainment of oscillation conditions dictated by the Barkhausen criterion[S4]. The open-loop measurements are performed by microwave network analysis between nodes 1 and 2 of the circuit. By setting the overall open-loop gain at the NEMS resonance frequency and its vicinity to be larger than 1 (*i.e.*, $|S_{21}| \geq 0$dB), and tuning the overall open-loop phase change to be $\phi(S_{21}) = 2n\pi$ (n is an integer), self-oscillation is realized when the loop is closed.

At stable self-oscillation, the frequency-domain oscillator output is characterized by using spectrum analyzer (HP8563E Spectrum Analyzer, 9kHz–26.5GHz). The time-domain oscillation waveforms are measured by employing a high-speed oscilloscope (Agilent Infinium 8000 Series Oscilloscope, 8GSa/s).

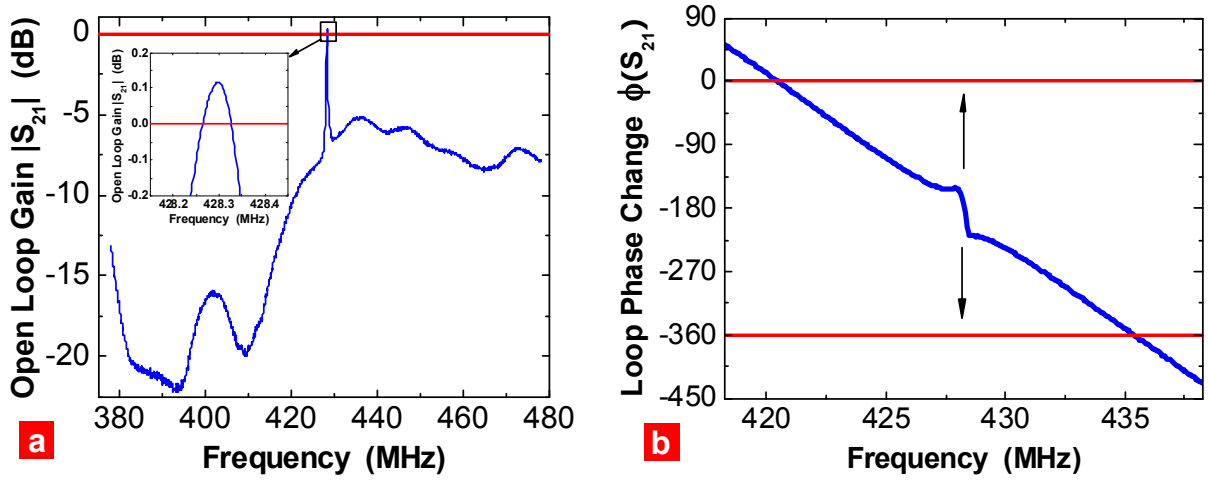

Figure S3 Open loop calibration and satisfying the Barkhausen criterion by adjusting **(a)** the open loop gain and **(b)** the loop phase change.

NEMS Oscillator Phase Noise and Frequency Stability: Comparison and Ultimate Limits

This section supplements the discussion covered in the main text, on the phase noise performance of our UHF NEMS oscillator. Here we show again in Fig. S4 the measured phase noise data with the Leeson-type empirical fit[S4,S5,S6], and the ultimate performance of this NEMS oscillator as limited by the device's thermomechanical fluctuations[S7]. Moreover, we amend the plot by incorporating some data from state-of-the-art 13MHz quartz crystal oscillators[S8], for comparison.

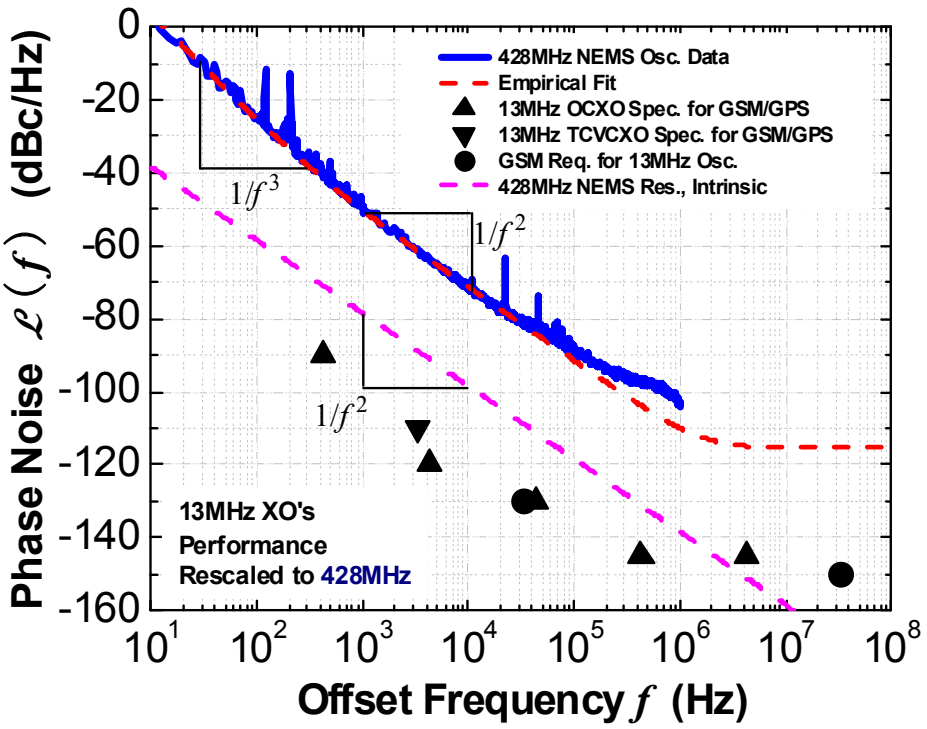

Figure S4 Phase noise performance of the UHF NEMS oscillator, in comparison with high-performance 13MHz quartz crystal oscillators (the phase noise performance is rescaled to the 428MHz carrier).

As also demonstrated in Fig. S4, it is noteworthy that the intrinsic noise limits of the NEMS oscillators yield frequency stability approaching that of the state-of-the-art quartz crystal oscillators (XO's)[S8]. This suggests potential high-profile future applications for NEMS oscillators such as GSM/GPS communications. The phase noise performance of the present unoptimized, prototype NEMS oscillator already matches or surpasses the levels achieved by oscillators based on doubly-clamped beam MEMS resonators[S9]. MEMS oscillators based on much stiffer micromechanical modes, in structures such as wine-glass disk resonators[S9], film-bulk acoustic resonators (FBAR's)[S10], have now being engineered to approach the phase noise performance of macroscale quartz crystal oscillators[S11]. We note that such phase noise comparisons require rescaling of different oscillators' performance with respect to their carrier frequencies, so that a common figure of merit is evaluated and fairly compared[S1]. While the MEMS resonators can handle carrier signal power (P_C) in the range of ~0.1μW to ~1mW (for devices ranging from doubly-clamped beams to wine-glass disks and to FBAR's), the power handling of UHF NEMS resonators (doubly-clamped beams) is often in the range of P_C~0.1nW–100nW[S1]. We also note that in the comparison of phase noise performance in Fig. S4, the NEMS oscillator performance is associated with a lower temperature. At elevated temperatures, thermomechanical noise and Johnson noise rise but this temperature effect is minor; the amplifier noise is relatively temperature insensitive (determined by the amplifier's equivalent noise temperature or noise factor).

The ultimate, intrinsic phase noise limits for NEMS may also be attainable with advanced resonator designs to increase the device Q, and with the possible use of NEMS arrays to enhance power handling (P_C) and reduce noise. For example, a ten-fold improvement in Q, *i.e.*, to ~25,000 (assuming fixed resonance frequency and power handling) would yield $\langle \delta f_0 / f_0 \rangle_\tau$ ~

5×10^{-11}. Such benefits may be achievable with optimization of mode-shape designs (*e.g.*, using stiffer modes and minimizing clamping losses) and advanced device processing techniques (*e.g.*, employing materials with ideally-terminated surfaces and ultralow internal friction, possibly also subjected to post-processing annealing or reflow).

In this work, the phase noise measurements are carried out using a specialized phase noise analyzer (RDL NTS-1000B Phase Noise Analyzer). The time-domain frequency stability characteristics are studied by using a high-precision frequency counter (Agilent 53132A Universal Counter, with UHF and high-precision options).

References

S1. Feng, X.L. *Ph.D. Thesis*, California Institute of Technology (2007).

S2. Huang, X.M.H., Zorman, C.A., Mehregany, M. & Roukes, M.L. Nanodevice motion at microwave frequencies, *Nature* **421**, 496 (2003).

S3. Huang, X.M.H., Feng, X.L., Zorman, C.A., Mehregany, M. & Roukes, M.L. VHF, UHF and microwave frequency nanomechanical resonators, *New J. Phys.* **7**, 247 (2005).

S4. A. Hajimiri, T.H. Lee, *The Design of Low Noise Oscillators* (Kluwer Academic Publishers, Norwell, 1999).

S5. Lee, T.H. & Hajimiri, A. Oscillator phase noise: a tutorial, *IEEE J. Solid-State Circuits* **35**, 326-336 (2000).

S6. Leeson, D.B. A simple model of feedback oscillator noise spectrum, *Proc. IEEE* **54**, 329-330 (1966).

S7. Cleland, A.N. & Roukes, M.L. Noise processes in nanomechanical resonators, *J. Appl. Phys.* **92**, 2758-2769 (2002).

S8. Phase noise data and specifications of the state-of-the-art quartz crystal oscillators as frequency references are from Raltron (www.raltron.com). GSM stands for global system for mobile communication, and GPS stands for global positioning system. OCXO stands for oven-controlled crystal oscillator and TCVCXO stands for temperature-compensated and voltage-controlled oscillator. For a fair comparison, data from the 13MHz quartz crystal oscillators are rescaled up to 428MHz by normalizing offset frequency to carrier frequency.

S9. Lin, Y.W. *et al.* Series-resonant VHF micromechanical resonator reference oscillators, *IEEE J. Solid-State Circuits* **39**, 2477-2491 (2004).

S10. Otis, B.P. & Rabaey, J.M. A 300μW 1.9GHz CMOS oscillator utilizing micromachined resonators, *IEEE J. Solid-State Circuits* **38**, 1271-1274 (2003).

S11. Vig, J.R. & Kim, Y. Noise in microelectromechanical system resonators, *IEEE Trans. Ultrason. Ferroelectr. Freq. Contr.* **46**, 1558-1565 (1999).